This is a peer-reviewed, accepted author manuscript of the following research article: Liu, C., Wang, K., Zhao, X., Chen, Z., Yin, X., Cai, T., Zhang, X., Xu, J., Hu, J., Meng, X., Ragauskas, A. J., & Jiang, J. (2023). Integrated lignocellulosic biorefinery for efficient production of furans and photothermal materials. *Chemical Engineering Journal*, *453*(Part 1), [139688]. https://doi.org/10.1016/j.cej.2022.139688

# Integrated lignocellulosic biorefinery for efficient production of furans and photothermal materials

Chao Liu [a, b], Kui Wang[a, b] *, Xinpeng Zhao[c], Zhijun Chen[c] *, Xiaoyan Yin[a], Tingting Cai[a], Xiaolei Zhang[d], Junming Xu[a, b], Jun Hu[e], Xianzhi Meng [f], Arthur J. Ragauskas[f, g, h] *, Jianchun Jiang[a, b] *

[a]*Institute of Chemical Industry of Forest Products, Chinese Academy of Forestry; Key Lab. of Biomass Energy and Material, Jiangsu Province; National Engineering Lab. for Biomass Chemical Utilization, Nanjing 210042, China*

[b]*Co-Innovation Center of Efficient Processing and Utilization of Forest Resources, Nanjing Forestry University, Nanjing 210037, China*

[c]*Engineering Research Center of Advanced Wooden Materials and Key Laboratory of Bio-based Material Science & Technology Ministry of Education, Northeast Forestry University, Harbin 150040, China.*

[d]*Department of Chemical and Process Engineering, University of Strathclyde, Glasgow G1 1XJ, UK*

[e]*School of Chemical Engineering, Northwest University, Xi'an 710069, China*

[f]*Department of Chemical and Biomolecular Engineering, University of Tennessee, Knoxville, Tennessee 37996, USA*

[g]*Joint Institute of Biological Sciences, Biosciences Division, Oak Ridge National Laboratory, Oak Ridge, Tennessee 37831, USA*

[h]*Center for Renewable Carbon, Department of Forestry, Wildlife, and Fisheries, University of Tennessee Institute of Agriculture, Knoxville, Tennessee 37996, USA*

[*]*Corresponding author emails: jiangjc@icifp.cn , wangkui@caf.ac.cn , chenzhijun@nefu.edu.cn , aragausk@utk.edu*

## Abstract

Integrated lignocellulosic biorefineries offer a great potential to valorize all the components in lignocellulose into products, including fuels, chemicals, and materials. However, because of lignocellulose recalcitrance, conversion of bioresources remains a techno-economic challenge for many lignocellulosic biorefineries. In this work, we have proposed a sustainable and profitable biorefinery strategy for lignocellulose fractionation and conversion. In this design, a biphasic solvent consisting of a molten salt hydrate $LiCl{\cdot}4H_2O$ and γ-valerolactone (GVL) was initially used for separating hemicellulose from lignocellulose. More interestingly, 100 wt% of biorefinery products

from lignin were directly converted to functional photothermal materials by coordinating with $Fe^{3+}$ for solar-thermal-electricity conversion. Attributed to this rational design, the techno-economic analysis predicts a revenue of 439.3 USD by processing 100 kg of lignocellulosic biomass using the above developed method.

**Keywords:** lignocellulosic biomass, molten salt hydrate, solvent effects, photothermal materials

## 1. Introduction

The core of the chemical industry is the conversion of petroleum resources into value-added products, including fuels, platform chemicals, polymers, materials and pharmaceuticals [1-3]. In the last century, fossil resources have constituted the primary feedstock for a multitude of chemical processes and transformations [4-6]. However, sustainability is becoming a global imperative due to the considerable depletion of fossil resources and environmental concerns [7, 8]. As a result, the biorefinery paradigm has been proposed as a solution for sustainable development [9, 10]. In a biorefinery, sustainable biomass feedstocks are refined/upgraded to energy products, polymeric materials, platform chemicals, and functional materials. Lignocellulose bioresources, due to their abundance and renewability, are regarded as one of the most promising sources for biorefineries [11-13]. Lignocellulose is primarily composed of cellulose (35-50%), hemicellulose (25-30%), and lignin (15-30%) [14-16]. Amongst them, cellulose and hemicellulose have been shown to exhibit potential as raw resources for HMF, levulinic acid, furfural and other furan derivatives [17-19]. Lignin is frequently proposed as a suitable source for guaiacol, phenol, phenolic resins, and other functional

materials [20-23]. The traditional lignocellulose biorefinery is heavily cellulose-centered, and it faces significant challenges nowadays [24]. To obtain readily hydrolysable cellulose, lignocellulose is often delignified initially prior to enzymatic hydrolysis, employing high pretreatment severities. In this process, a major part of hemicellulose could be lost especially under acidic conditions. Equally concerning, the extracted lignin often contains relatively inert C-C interunit linkages, rendering a low-value lignin resource for producing aromatic compounds [25, 26]. To address this problem, the lignin-first biorefinery was proposed as described in two works by Abu-Omar and Sels's group in 2015 [27, 28]. In this strategy, lignin is initially dissolved and depolymerized to yield phenolic/aromatic monomers, dimers, and oligomers, while cellulose and hemicellulose are retained in the solid residue for further treatment (e.g., enzymatic hydrolysis). This strategy represents significant progress in an integrated lignocellulose biorefinery, and for a more elaborate discussion on the development and guidelines of the lignin first approaches, the reader is referred to these dedicated studies and reviews [29-31]. Nevertheless, several critical challenges remained in the proposed process. Firstly, although the lignin-derived bio-oil has great potential, applications are still limited by the complicated isolated components. Moreover, a large amount of hemicellulose is lost or isomerized in lignin-first biorefinery, preventing their further conversion to chemicals [32, 33]. These considerations, combined with low efficient recovery of expensive catalysts, rendered a reduced efficiency and techno-economic balance for a cost-effective integrated lignocellulose biorefinery.

To address these issues, we have proposed a sustainable and profitable biorefinery

strategy (**Figure. 1**). In this design, a recyclable biphasic solvent system consisting of a molten salt hydrate ($LiCl{\cdot}4H_2O$) and biomass-derived γ-valerolactone (GVL) solvent was used for hemicellulose fractionation from lignocellulose with a separation efficiency of 93.2 wt%. After that, 90.5 wt % of cellulose and 88.7 wt% of lignin were separated from the solid residue using isopropanol/formic acid. As-obtained hemicellulose and cellulose were subsequently converted to furfural and HMF with a conversion yield of 76.2 mol% and 77.9 mol% in the biphasic solvent, respectively, catalyzed by $Al_2(SO_4)_3$. Finally, the lignin fraction was hydrogenized to phenolic monomers and oligomers. Instead of separating and purifying the phenolic mixtures, nearly 100 wt% of them were directly converted to functional photothermal materials by coordinating with $Fe^{3+}$ for solar-thermal-electricity conversion. Attributed to the rational design, techno-economic analysis suggests a revenue of 439.3 USD by processing 100 kg of lignocellulose using the as-developed method.

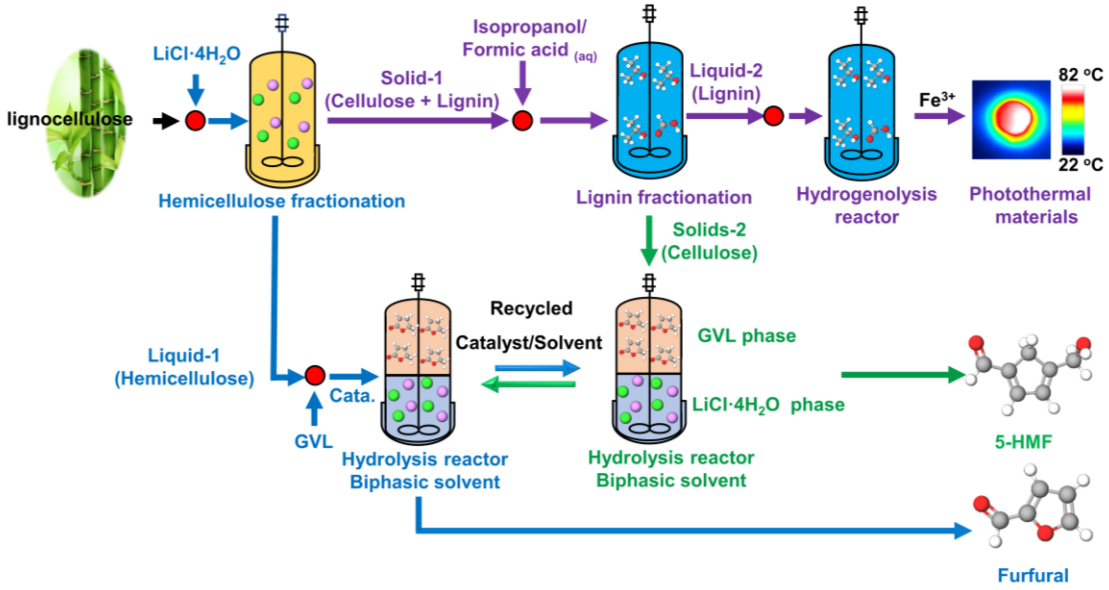


**Figure. 1.** Comprehensive catalytic strategy for lignocellulose powder full-component conversion.

# 2. Experimental section

## *2.1. Chemicals*

Bamboo was purchased from a farm (Sichuang, China), which was ground and sieved to average particle size of 50 μm prior to use. The chemical composition (wt%) of the pubescens was 40.5 % cellulose, 32.8 % hemicellulose, 23.2 % acid insoluble lignin and 2.6 % acid soluble lignin. The composition (wt%) of the pubescens was determined according the method of National Renewable Energy Laboratory (NREL, 2008a, Preparation of samples for Compositional Analysis; 2008b, Determination of Structural Carbohydrates and Lignin in Biomass.). LiCl, $Al_2(SO_4)_3$, formic acid and microcrystalline cellulose were purchased from Sinopharm Chemical Reagent Co. γ-valerolactone and isopropanol were got from Aladdin Reagent Co. Guaiacol, 4-ethylguaiacol, 2-methoxy-4-methylphenol, syringic acid, 2,6-dimethoxy-4-methylphenol, 2,6-dimethoxyphenol, 4-methylphenol, phenol, syringaldehyde, 2-methoxy-4-propylphenol, 4-ethylphenol, eugenol and 4-hydroxy-3-methoxyacetophenone were supplied by Sigma-Aldrich company. Commercial 5 wt% Ru/C, Pt/C, Pd/C and Rh/C catalyst were purchased from Shanghai Macklin Biochemical Co., Ltd. All chemicals were analytical grade and used as received without further purification.

## *2.2. Preparation of molten salt hydrate*

The purchased LiCl and deionized water were mixed according to the required water/salt molar ratio, then added to a 500 ML 316L stainless steel autoclave with Teflon lining, followed by stirring (800 rpm) at 60 °C for 30 min. The $LiCl{\cdot}4H_2O$ was obtained after cooling to room temperature.

### *2.3. Hemicellulose fractionation and hemicellulose-to-furfural conversion*

Typically, 3.0 g bamboo and 20.0 g $LiCl·4H_2O$ were added into a 50 mL 316L stainless steel autoclave with Teflon lining, followed by stirring at 800 rpm. Then, the reactor was pressurized by 2 Mpa of $N_2$ and heated at 130 °C for 60 min. The zero time was defined as the mixed reaction solution reaches the target temperature. Upon completing the reaction, the reactor was rapidly cooled in an ice bath, and the mixture was filtered through a 0.45 μm membrane to collect the solid and liquid products. The main components of the solid product are cellulose and lignin, which were defined as **Solid-1** (1.9 g). The solid products were washed 3-5 times with deionized water, freeze-dried, and stored in a constant temperature drying oven for further treatment. The liquid products were defined as **Liquid-1** (21.1 g, containing hemicellulose-derived oligomers). Additionally, the above-obtained **liquid-1**, 10.0 g GVL and 0.1 g $Al_2(SO_4)_3·18H_2O$ were added to a 50 mL 316L stainless steel autoclave with Teflon lining. $N_2$ was charged into the reactor at an initial pressure of 2.0 MPa to remove air, followed by programmed heating (heating rate =7.5 °C/min) up to the target temperature (120–170 °C) and stirring with 800 rpm for a period of time (15–90 min). The products were analyzed by GC-MS and HPLC.

$$\text{Furfural yield} = \frac{\text{mole of furfural}}{\text{mole of hemicellulose}} \times 100\%$$

$$\text{Energy consumption (kWh)} = \text{p (kW)} \times \text{t (h)}$$

### *2.4. Lignin fraction and Lignin depolymerization*

The above-obtained **Solid-1**, 3.0 g formic acid, 20.0 g isopropanol and 20.0 g $H_2O$ were added to a 100 mL 316L stainless steel autoclave with Teflon lining, followed by stirring

speed was fixed at 800 rpm. Then, the reactor was pressurized by 2 MPa of $N_2$ and heated at 160 °C for 60 min. After the reaction was completed, the reactor was rapidly cooled in an ice bath, and the mixture was filtered through a 0.45 μm membrane to collect the solid and liquid products. The main component of the solid product is cellulose, which was defined as **Solid-2** (1.08 g, rich in cellulose). The solid products were washed 3-5 times with deionized water, freeze-dried, and stored in a constant temperature drying oven for further treatment. The liquid products were defined as **Liquid-2** (43.8 g, contains lignin-derived oligomers). Furthermore, the above-obtained **Liquid-2** and 0.2 g commercial catalyst (e.g., Ru/C) were put together in a 100 mL 316L stainless steel autoclave with Teflon lining, followed by stirring speed was fixed at 800 rpm. Then, the reactor was pressurized by 2 Mpa of $H_2$ and heated at 210 °C for 4.0 h. After reaction, the reactor was rapidly cooled down in an ice bath, and the mixture was filtered through a 0.45 μm membrane to collect the catalyst and liquid products. The liquid product is qualitatively and quantitatively analyzed by GC-MS and GC.

### *2.5. Depolymerized lignin-to-photothermal materials conversion*

1.2 g of hydrogenolyzed lignin was dissolved in 15.0 mL of ethanol. A sodium hydroxide solution (10.0 mL, pH=12) was the added. The solution was stirred for 10 min, then an aqueous solution containing 0.4 g of ferric chloride was added (5.0 mL). The mixed solution was stirred for 10 min and freeze-dried to give a solid powder (~1.6 g).

### *2.6. Cellulose-to-HMF conversion*

0.54 g of the above-obtained **Solid-2** (Contains 0.5g of cellulose), 10.0 g $LiCl{\cdot}4H_2O$,

20.0 g GVL, and 0.05g $Al_2(SO_4)_3$ were placed in a 100 mL 316L stainless steel autoclave with Teflon lining, followed by stirring speed was fixed at 800 rpm. It should be noted that the solvent and catalyst can be fresh or recycled. Then, the reactor was pressurized by 2 MPa of $N_2$ and heated at 160-200 °C for 60-120 min. Zero time was defined as the mixed reaction time for the solution to reach the target temperature. After the reaction, the reactor was rapidly cooled in an ice bath, and the mixture was filtered through a 0.45 μm membrane to collect the solid and liquid products. The liquid product is qualitatively and quantitatively analyzed by GC-MS and GC.

### *2.7. Computational simulations*

Forcite and CASTEP module of the Materials Studio software was employed for the quantum chemistry calculations. In the molecular dynamics calculations, liquid-phase molecular systems were prepared by placing a reaction molecule, solvent molecules in a nearly 50×50×50 periodic box to simulate the effect of ratios between $LiCl·4H_2O$ and GVL on the reaction, where the number of reactants is constant, and the solvent molecules were changed to simulate the concentrations. The operating temperature is set at 413 K and controlled by means of the Nose thermostat method to match the actual experimental procedure. The prepared molecular systems were equilibrated for 1 ns by NVT (constant molecule numbers, volume, and temperature) ensemble. The Van der Waals interaction is calculated by atom-based method with a cutoff radius of 18.5 Å to avoid the errors of relatively short-range non-bond interactions, while electrostatic summation is calculated by Ewald method to avoid the errors of long-range non-bond energy in periodic systems.

Activation free energy are calculated by the following equation：

$$\Delta E = E[Product] - E[Reaction]$$

where E[Product] and E[Reaction] is the energy of single molecule after optimized in corresponding solution; For example, the activation free energy from Cellulose to Glucose is calculated by E[Glucose] - E[Cellulose].

### *2.8. Product analysis*

FAL and 5-HMF in the GVL was analyzed by gas chromatography (GC, 2010Plus, Shimadzu) for qualitative and quantitative tests. The gas chromatograph uses the SH-RTX-5 column (30m×0.32mm×0.5um), and the flame ionization detector (FID) were used to determine the volatile components with 0.43 mL $min^{-1}$ of gaseous helium as the carrier gas. The temperature of the injector was set to 260 °C, and the temperature of the detector was 280 °C. The column temperature programming was adopted as follows: The initial temperature of the chromatographic column was set at 100 °C for 2 min, then heated up to 280 °C at the rate of 8.0 °C $min^{-1}$, and held at 280 °C for 10 min. Likewise, phenolic monomers are detected with the above-mentioned gas phase equipment. The initial temperature of the chromatographic column was set at 50 °C for 2 min, and the oven temperature program was raised with a ramp of 20 °C $min^{-1}$ from 50 °C to 280 °C for 5 min. The injector and detector temperatures was kept at 275 °C and 280 °C, respectively. Besides, the FAL, 5-HMF and sugars in water phase were measured by HPLC (Agilent 1200 series) equipped with an amines column (Model HPX-87H, 300 mm×7.8 mm, Bio-Rad), a variable-wavelength detector (Model VWD-3×00(RS)), and a refractive index (RI) detector (Model RI-101, Shodex). The mobile

phase was 5 mM $H_2SO_4$ at a flow rate of 0.6 mL/min. The temperature of the detector and column oven was maintained at 35 °C and 50 °C, respectively. Moreover, the chemical composition of HDO is determined by Anion Exchange Chromatography (HPACE, Dionex ICS-3000) equipped with a Carbopac PA-100 column (4×250 mm, Dionex), the mobile phase is 150 mM sodium hydroxide solution containing 100 mM sodium acetate, the flow rate is 0.4 mL/min, and the column temperature is 30 °C.

### *2.9. Characterization of Solid-2 and microcrystalline cellulose*

The crystallinity of the sample was analyzed with an X-ray diffractometer (XRD) at 30 mA and 40 kV, respectively, the scanning rate was 5 °/min, and the scanning range was 5° to 50°. The crystallinity index (CrI) is calculated as follows:

$$CrI=\frac{I_{002}-I_a}{I_{002}}\times 100\%$$

$I_{002}$ represents the diffraction intensity of the crystalline region (2θ = 22.5°) of cellulose in the biomass component; Ia represents the diffraction intensity of the amorphous region (2θ = 18.5°) of cellulose in the biomass component.

The composition and structure of the substrates and residues were determined by a PerkinElmer Spectrum One Fourier transform infrared spectroscope (FTIR). The attenuated total reflectance (ATR) method was adopted here over the scan area range from 4000 to 500 $cm^{-1}$with resolution of 4 $cm^{-1}$ and accumulation of 4 times.

### *2.10. Characterization of Liquid-1 and hydrogenolysis products*

Molecular weights of the Liquid-1 and hydrogenolysis products were measured by gel permeation chromatography (GPC). The instrumentused was a Waters high-performance liquid chromatography with a refractive index (RI) detector. The mobile

phase is THF, and the constant column temperature is 30 °C. A calibration curve was acquired by polystyrene as standards.

## 3. Results and Discussion

### *3.1. Step 1: Hemicellulose-to-furfural conversion*

The hemicellulose fractionation from the native plant cell wall and its subsequent conversion to furfural are illustrated in **Figure. 2a**. Specifically, 93.2 wt% of hemicelluloses were separated from biomass at optimized conditions (130 °C for 60 min) in molten $LiCl{\cdot}4H_2O$ (**Figure. 2b**). Meanwhile, the molten salt hydrate $LiCl{\cdot}4H_2O$ showed good selectivity as a hemicellulose solvent, while 90.1 wt% of cellulose and 96.3 wt% of lignin were not dissolved and remained in Solid-1 for further separation. This result may be attributed to the following two points: 1) Metal cations can promote the break of glycosidic bonds and melt salt hydrate has a good dissolution effect on hemicellulose and cellulose[34, 35]; 2). Cellulose is encapsulated in hemicellulose and lignin and has a dense crystalline structure, so it has higher stability than hemicellulose and requires more demanding reaction conditions for dissolution/degradation[36, 37]. High-performance anion exchange chromatography (HPACE) and liquid chromatography (HPLC) were used to determine the components in **Liquid-1** [38] . The results showed that the main components of **Liquid-1** are oligosaccharides (40.79 wt%, derived from hemicellulose), xylose (36.26 wt%), furfural (13.13 wt%), glucose (5.54 wt%), and others (4.28 wt%, *e.g.,* acetic acid, arabinose and galactose) (**Figure. 2c**). Subsequently, GVL aqueous solution was added to the **Liquid-1** to form a biphasic solvent for the subsequent catalytic reactions. $Al_2(SO_4)_3$ was then added to the biphasic

solvent as a catalyst. A 76.2 mol% of furfural conversion in the biphasic solvent was achieved under optimized conditions (150 °C for 45 min), which is comparable to the maximum xylan-to-furfural conversion yield, but significantly less process time (**Figure. 2d**). As a control, only 37.6 mol% (150 °C for 60 min) of furfural conversion was achieved in the presence of $Al_2(SO_4)_3$ without the addition of GVL (**Figure. S1**). The result was attributed to the fact that GVL could provide a protective shell for furfural to avoid its condensation, thus having a positive effect on furfural production[39]. A plausible conversion mechanism was then proposed. $Al_2(SO_4)_3$ is simultaneously hydrolyzed to $H^+$ and Lewis acid catalytic active center $[Al(OH)_2(aq)]^+$ in $LiCl \cdot 4H_2O$/GVL. Oligosaccharides in **Liquid-1/GVL** were then depolymerized to xylose under the acidic condition. Our previous studies showed that $[Al(OH)_2(aq)]^+$ could complex with the oxygen atoms of xylose at C1 and C2 position [40]. Such interactions accelerated hydrogen transfer between the two carbon atoms, followed by isomerization of xylose into xylulose. Meanwhile, $LiCl \cdot 4H_2O$ also showed catalytic performance converting xylose to xylulose. This synergistic catalytic effect of $LiCl \cdot 4H_2O$ and $Al_2(SO_4)_3$ enabled a high yield of furfural. In conclusion, oligosaccharides and xylose in **Liquid-1** were converted to sugar intermediates catalyzed by $LiCl \cdot 4H_2O$ and $Al_2(SO_4)_3$, which subsequently yielded furfural (**Figure. 2f**). The accumulated furfural was solubilized in GVL layer, which significantly alleviated the side reactions of sugar intermediates and resulted in a high conversion yield[41, 42]. To investigate its potential in a practical application, catalyst and solvent recycling experiments were conducted. Firstly, $Al_2(SO_4)_3$ is insoluble in $LiCl \cdot 4H_2O$ at room temperature, thus it

could be easily separated from the reaction mixture by filtration. GVL on the upper layer was recycled by removing furfural via a vacuum distillation. $LiCl{\cdot}4H_2O$ was recovered by employing the activated carbon to adsorb the incorporated byproducts [43]. It was shown that the recycled solvent did not show an obvious change in performance in separating hemicellulose and hemicellulose conversion after three cycles, when compared with the original solvent and catalyst (**Figure. 2e**).

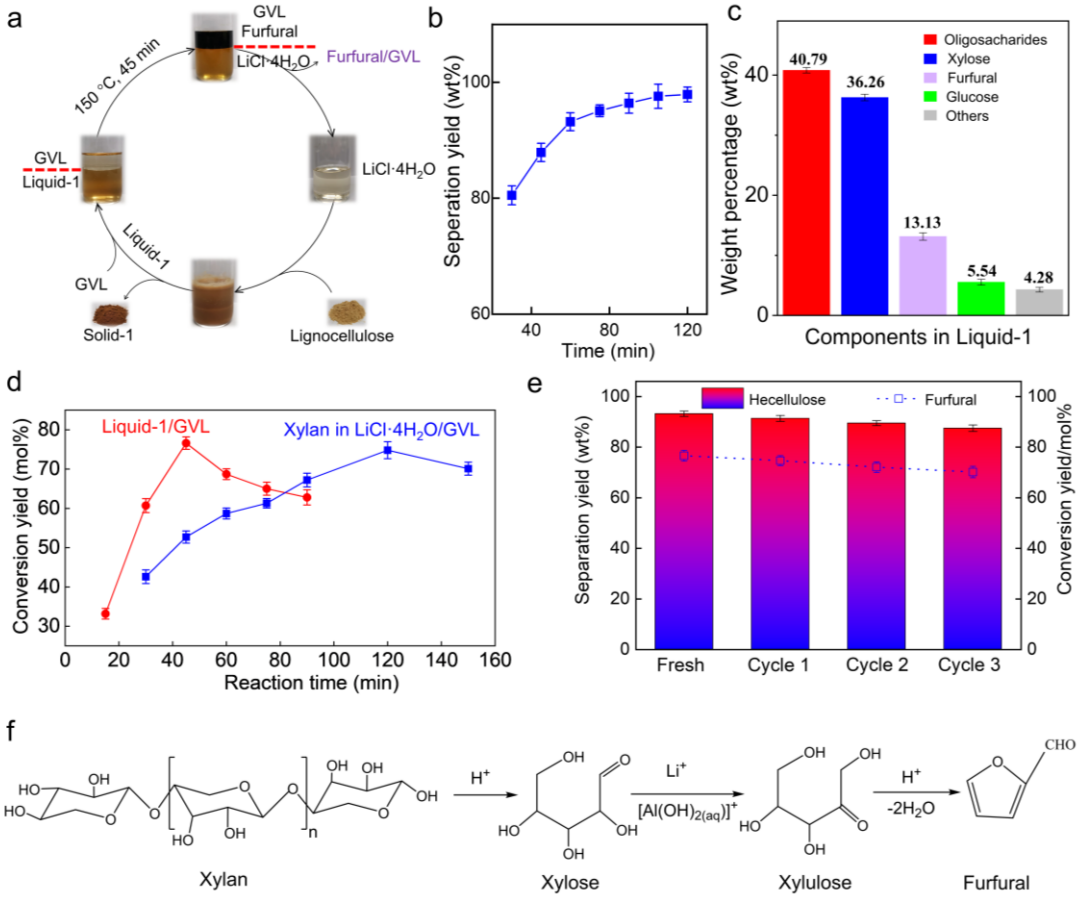


**Figure. 2. Hemicellulose fractionation and conversion.** a) Schematic illustration of hemicellulose fractionation and conversion. b) Weight percentage of fractionated hemicellulose from lignocellulose at different reaction times, reaction conditions: 3.0 g bamboo, 20.0 g $LiCl{\cdot}4H_2O$, 2 Mpa $N_2$, 130 ºC. c) Components in fractionated hemicellulose. d) Conversion yield of Liquid-1/GVL and Xylan in $LiCl{\cdot}4H_2O$/GVL to furfural at different times, reaction conditions: 21.1 g Liquid-1or 0.89 g xylan, 2 Mpa $N_2$, 10.0 g GVL at 150 ºC catalyzed by 0.1 g$Al_2(SO_4)_3$, calculation based on the hemicellulose in the lignocellulose. e) Reusability of the biphasic system (GVL/$LiCl{\cdot}4H_2O$) and $Al_2(SO_4)_3$, the reaction parameters were consistent with the corresponding reaction steps above. f) Hydrolysis of xylan to furfural.

### *3.2. Step 2: Lignin-to-photothermal materials conversion*

After hemicellulose fractionation, lignin was separated from **Solid-1** (Detailed chemical components shown in Table S1) and depolymerized to a bio-oil (**Figure. 3a**). Three main steps are involved: (i) lignin dissolution and cellulose separation; (ii) lignin hydrogenolysis; and (iii) solvent and catalyst recovery. In the first step, **Solid-1** was treated with isopropanol/formic acid (aq). 89 wt% of lignin was dissolved in the solvent while most of cellulose (90.5 wt%) precipitated in solid state. After removing cellulose via filtration, the lignin solution (**Liquid-2**) was hydrogenized assisted by various catalysts *(e.g.*, Pd/C, Pt/C, Rh/C, and Ru/C). A crude oil, which consists mainly of phenolic compounds, was obtained after recovering catalyst and isopropanol/formic (aq) via simple liquid/solid separation and flash evaporation. GC-MS analysis showed that Ru/C showed the best catalytic performance (**Table S2**). The conversion yield of mono- and oligo- phenolics was 71.2 wt% (**Figure. 3b**). GPC analysis showed that the Mw/Mn of lignin (in Liquid-2) decreased from 1298/786 Da (Mw > 600 Da accounting for 56.7%) to 916/575 Da (Mw > 600 Da accounting for 15.0%) (**Figure. 3b**). These results suggested that lignin was efficiently converted into phenolic monomers/oligomers catalyzed by Ru/C. It is worth noting that Ru/C still showed satisfactory catalytic activity after 5 cycles (**Figure S2**). The recovered monomer-/oligomer- phenolics were fully converted to photothermal reagents via coordinating with $Fe^{3+}$. As shown in **Figure S3 a-c**, the photothermal material is a crystal with obvious granular surface and rich in hydroxyl group. UV-vis-NIR **(Figure S3d)** verified the following characteristics of photothermal materials: 1) Extremely wide absorption spectra covering the whole

311 solar spectrum; 2) photothermal materials showed absorbance over a wide range of
312 wavelengths (200−2000 nm), which overlaps well with the solar spectrum; 3) It shows
313 strong absorption throughout the solar spectrum. These results show that the prepared
314 photothermal materials have excellent solar energy absorption capacity. By promoting
315 the absorbance and non-radiative migration of phenolics, such phenolics-iron complex
316 showed an efficient photothermal conversion [44]. The temperature of the photothermal
317 reagents increased from 24 ºC to 79 ºC during 15 min irradiation, suggesting that the
318 material is able to carry out efficient photothermal conversion (**Figure. 3c**). The effect
319 of irradiation on the materials was reversible, and there was no noticeable change in
320 photothermal conversion after five cycles (**Figure. 3d**). Encouraged by these results,
321 we then investigated the possibility of using the photothermal reagents to drive a
322 thermoelectric generator. Photothermal reagents, a thermoelectric module, and a
323 cooling system were combined to create a solar-powered thermoelectric generator. The
324 photothermal reagents absorbed simulated solar light (100 mW $cm^{-2}$) and heated the
325 thermoelectric module on one side, creating a temperature difference from the other
326 side nearest to the cooling system, and generating a voltage of 0.25 V (**Figure. 3e**).
327 Further increasing the mimetic solar intensity to 200 mW $cm^{-2}$ and 300 mW $cm^{-2}$
328 triggered a voltage output of 0.35 V and 0.40 V, respectively. The as-prepared
329 thermoelectric generator was sensitive to photo irradiation. Switching off the light
330 source immediately reduced the voltage generated by the thermoelectric generator
331 (**Figure. 3e**), demonstrating good controllability of the device. The voltage output did
332 not show obvious change after 5 cycles of switching on/off the solar sources, suggesting

the superior stability of such solar-thermal-electricity conversion (**Figure. 3f**). More interestingly, a motion of engine was triggered by as-prepared solar-driven thermoelectric generators (**Figure. 3g** and **Video S1**).

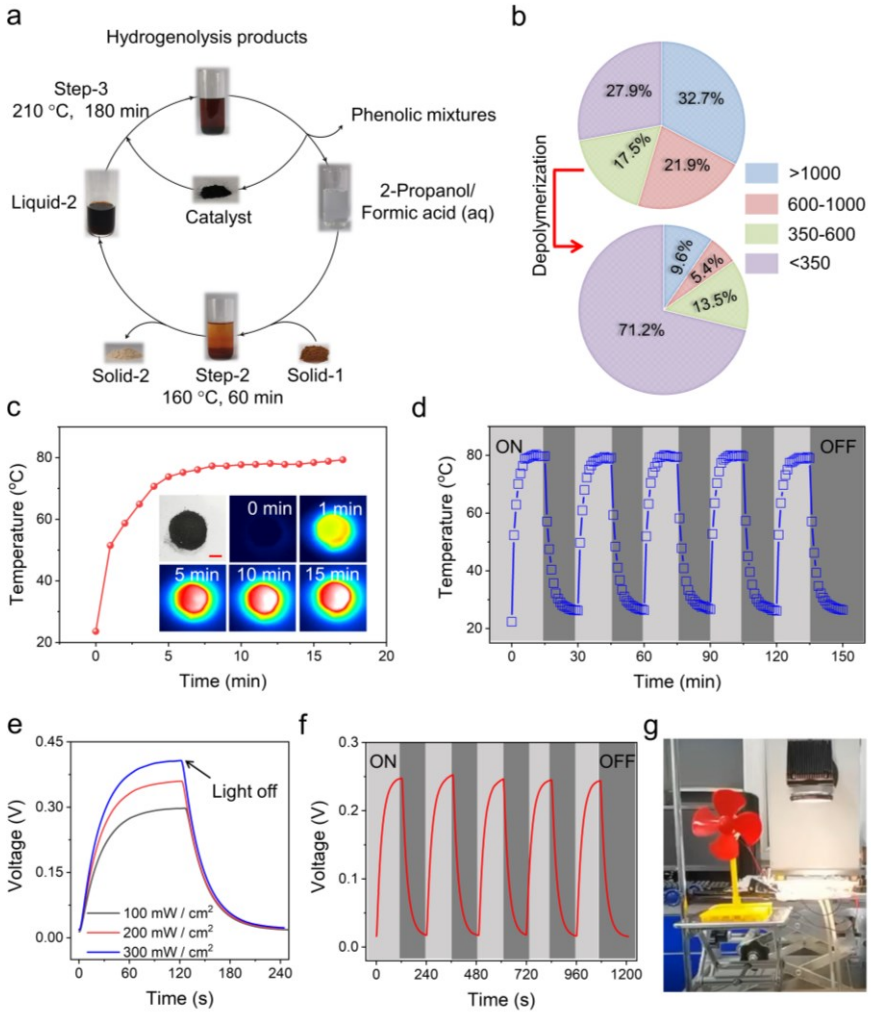


**Figure. 3**. **Depolymerization of lignin and functional conversion.** a) Schematic illustration of lignin fractionation and depolymerization. b) The components of lignin and depolymerized lignin, reaction conditions: 43.8 g Liquid-2, 0.2 g Ru/C, 2 Mpa $H_2$, 210 ℃ for 4 h. c) Temperature changes of depolymerized lignin-derived photothermal materials, inset: the digital and IR images of depolymerized lignin-derived photothermal materials upon mimetic solar irradiation (100 mW $cm^{-2}$), scale bar = 1 cm. d) Recycled temperature changes of depolymerized lignin-derived photothermal materials upon switching on/off mimetic solar irradiation (100 mW $cm^{-2}$). e) Voltage output of thermoelectric generators upon switching on/off mimetic solar irradiation at different intensities. f) Recycled voltage changes of thermoelectric generators upon switching on/off mimetic solar irradiation (100 mW $cm^{-2}$). g) Digital images of fans driven by thermoelectric generators upon mimetic solar irradiation, scale bar = 2 cm.

### *3.3. Step 3: Cellulose-to-HMF conversion*

Cellulose-rich **Solid-2** (92.2 wt%) was obtained after lignin fractionation from **Solid-1** (**Figure. 4a**). **Solid-2** was further explored for its conversion to HMF in $LiCl{\cdot}4H_2O$/GVL. Catalyzed by the recycled $Al_2(SO_4)_3$ from the hemicellulose conversion step, up to 77.9 mol% conversion yield of HMF was achieved (170 °C for 90 min) (**Figure. 4b**). As obtained HMF was well dissolved in the upper GVL layer and could be easily obtained via a simple distillation. In order to explore the mechanism for such high conversion yield, product evolution was analyzed. Glucose and fructose were observed as intermediates in the reaction (**Figure. S4**), indicating that the reaction has undergone cellulose hydrolysis, glucose isomerization, and fructose dehydration [45, 46]. To further explore the reaction mechanism, several control experiments were conducted. In the molten salt hydrate $LiCl{\cdot}4H_2O$ solvent without $Al_2(SO_4)_3$, a 26.8 wt% conversion yield of glucose was achieved (**Figure. S5**). Most of the glucose existed in the $LiCl{\cdot}4H_2O$, and no glucose was observed in GVL (**Figure. S6**). In contrast, only 5.3 wt% conversion yield of glucose was produced in $Al_2(SO_4)_3$ aqueous without the $LiCl{\cdot}4H_2O$ at the same condition (**Figure. S7**). These results suggested that depolymerization of cellulose is mainly promoted by $LiCl{\cdot}4H_2O$ rather than $Al_2(SO_4)_3$ and GVL. Moreover, 8.2 wt% and 23.7 wt% of fructose were obtained in the molten $LiCl{\cdot}4H_2O$ and $Al_2(SO_4)_3$ aqueous, respectively. Similarly, no fructose was detected in GVL (**Figure. S6**). These results suggest that the isomerization of glucose to fructose is mainly catalyzed by $Al_2(SO_4)_3$. Furthermore, only a trace amount of HMF loss and no structural change was observed when HMF was dissolved in GVL upon heating at

170 ºC for 20 min, indicating that GVL efficiently stabilized as-produced HMF in the reaction system (**Figure. S8**). In summary, the mechanism for converting cellulose to HMF in the biphasic solvent was proposed. Cellulose was first depolymerized to yield glucose assisted by the molten $LiCl·4H_2O$. After which, $Al_2(SO_4)_3$ triggered the isomerization of glucose to fructose, which dehydrated to give HMF. The produced HMF then entered the upper GVL layer and was efficiently dissolved in this layer (**Figure. 4c**). The effect of ratios between $LiCl·4H_2O$ and GVL on the reaction was also investigated. The sequence of HMF yields in different reaction media is as follows: 77.9 mol% (10/20, $LiCl·4H_2O$ /GVL, g/g) > 74.6 mol% (5/25, $LiCl·4H_2O$ /GVL, g/g) > 66.5 mol% (15/15, $LiCl·4H_2O$ /GVL, g/g) > 42.8 mol% (20/10, $LiCl·4H_2O$ /GVL, g/g) (**Figure. 4d**). To understand such differences, molecular dynamics (MD) calculations were conducted to show the free energy of each intermediate for cellulose conversion. Glucose-fructose isomerization and cellulose-glucose depolymerization showed the biggest and the second biggest energy barrier, 11.9 KJ/mol and 9.8 KJ/mol, respectively, indicating these steps were the rate-limiting steps (**Figure. S9**). Further calculation results for the energy barrier values of the rate-limiting steps in reactions with different $LiCl·4H_2O$ /GVL ratios were as follows: -35.4 KJ/mol (10/20, $LiCl·4H_2O$/GVL, g/g) < 102.2 KJ/mol (5/25, $LiCl·4H_2O$ /GVL, g/g) < 119.7 KJ/mol (15/15, $LiCl·4H_2O$/GVL, g/g) < 123.8 KJ/mol (20/10, $LiCl·4H_2O$ /GVL, g/g) (**Figure. 4e**). Thus, the rate-limiting steps showed the lowest energy barrier when the weight ratio between $LiCl·4H_2O$ and GVL was 10:20. Such a low energy barrier was beneficial for the cellulose-HMF conversion and induced a high conversion yield. Interestingly, the conversion yield was

even higher than the value of microcrystal cellulose-to-HMF conversion (70.2 mol%) at the same condition. This effect was attributed to the lower crystallinity of cellulose in **Solid-2**, compared to the microcrystal cellulose, which was proved by XRD, FTIR, and FTIR (**Figure. S10**). The lower crystallinity facilitated accessibility of solvents and catalyst to the cellulose in **Solid-2,** which promoted the conversion. As a result, energy consumption analysis suggests that to produce a considerable amount of HMF, the energy consumed by microcrystal cellulose is 1.16 times (2.117 kWh) that of as-obtained cellulose (1.822 kWh) (**Figure. S11**).

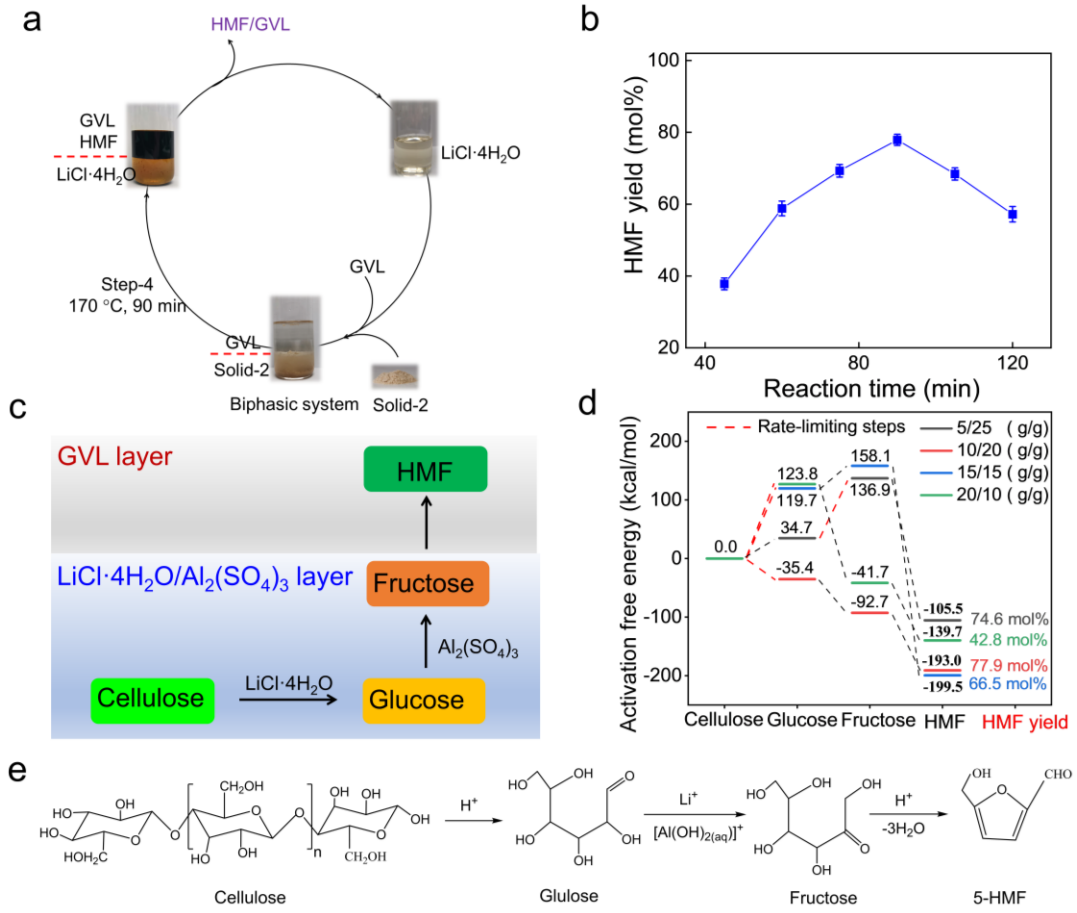


**Figure. 4**. **Cellulose-to-HMF conversion.** a) Schematic illustration of cellulose-to-HMF conversion. b) Conversion yield of HMF in LiCl·4H$_2$O/GVL at different times, reaction conditions: 0.54 g Solid-2, 10.0 g LiCl·4H$_2$O, 2 Mpa $N_2$, 20.0 g GVL, and 0.05g $Al_2(SO_4)_3$ at 170 °C catalyzed by $Al_2(SO_4)_3$. c) Proposed mechanism for Cellulose-to-HMF conversion in LiCl·4H$_2$O/GVL catalyzed by $Al_2(SO_4)_3$. d) The activation free energy profile of each reaction intermediate in a biphasic solvent. e)

Hydrolysis of cellulose to HMF.

### *3.4. Comprehensive mass balance of biorefinery strategy*

Based on the obtained experimental data, technical-economic was conducted on the integrated hemicellulose-first biorefinery (**Figure. 5a**). In the model process, 20.03 kg HMF, 10.2 kg furfural, 25.8 kg photothermal materials, 27.94 kg sugars derived (for bioethanol) and 14.33 kg $H_2O$ could be obtained from 100 kg lignocellulose. Market investigation showed that the price of HMF and furfural is 500.75 USD and 153.0 USD, respectively. The assumptions in the biorefinery are listed in **Table S3**. Labor cost (143.36 USD) is the biggest contributor to the costs. Due to the loss of formic acid recovery process, formic acid consumption section is the second highest contributor to the cost (~39.0 USD). It is worth noting that the value of lignin-derived photothermal materials is waiting for further evaluation. Overall, our proposed process can generate revenue of 439.3 USD by processing 100 kg of lignocellulose (**Figure. 5b**).

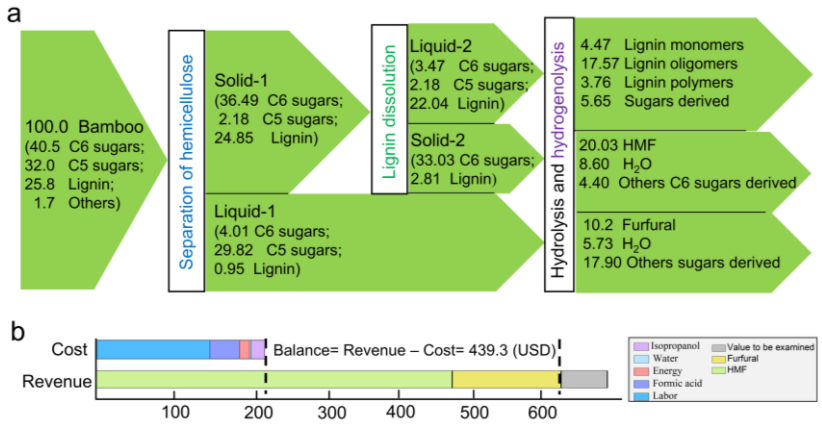


**Figure. 5. Mass balance and economics for the bamboo powder biorefinery strategy.** a) bamboo fractionation and full-component conversion process. b) costs and revenues. Reaction conditions: Separation of hemicellulose (130 °C for 1 h, 2Mpa $N_2$), Lignin dissolution (160 °C for 1 h, 2Mpa $N_2$), Hydrolysis (cellulose: 150 °C for 0.75 h, hemicellulose: 170 °C for 1. 5 h, 2 Mpa $N_2$), Hydrogenolysis (210 °C for 4 h, 2Mpa $H_2$).

## 4. Conclusion

In summary, we have proposed a sustainable and profitable biorefinery strategy in this

paper via a recyclable biphasic solvent ($LiCl{\cdot}4H_2O$/GVL). Hemicellulose, lignin, and cellulose were fractionated from lignocellulose at a high yield. Subsequently, the fractionated hemicellulose and cellulose showed high reactivity and can be efficiently converted to furfural and HMF, respectively. Moreover, depolymerized products from as-separated lignin were fully converted to photothermal materials by coordinating with iron ions for solar-thermal-electricity conversion without any separation and purification, which overcomes the limitations in traditional lignin biorefinery. The rational design enabled a revenue of 439.3 USD by processing 100 kg of lignocellulose. More importantly, all the catalysts and chemicals in the developed biorefinery are commercially available. As a result, our method is applicable and very promising in the practical industry. Generally, this work is expected to give a new strategy and practical solution to produce valuable chemicals and functional materials from lignocellulosic biorefinery

**Author contributions**

C.L. carried out the lignocellulose fractionation and depolymerization experiment. X.Z. performs photothermal reagent preparation experiment. J.H. and X.Z. perform molecular dynamics calculation experiment. X.Y. and T.C. perform the experiment of the chemical component of lignocellulose. C.L. wrote the manuscript assisted by K.W., Z.C. and X.M.; K.W., J.J. and A.J.R. conceived the work, and all authors discussed the experimental and analyzed the data. X.M. and A.J.R. efforts were funded by the University of Tennessee.

**Competing interests**

The authors declare no competing interests.

**Acknowledgements**

The authors would like to thank National Nature Science Foundation of China (31870714), and the Youth Talent Support Program for Science & Technology Innovation of National Forestry and Grassland (2019132603) for financial support. Natural Science Funding of Heilong Jiang province for Excellent Young Scholar (YQ2020C017). The work was carried out at Shanxi Supercomputing Center of China, and the calculations were performed on TianHe-2.

**Data availability:** The authors declare that all of the data that support the findings of this study are available within the article and its Supplementary Information files or from the corresponding author upon reasonable request.

## References

[1] A.W. Bartling, M.L. Stone, R.J. Hanes, A. Bhatt, Y. Zhang, M.J. Biddy, R. Davis, J.S. Kruger, N.E. Thornburg, J.S. Luterbacher, R. Rinaldi, J.S.M. Samec, B.F. Sels, Y. Román-Leshkov, G.T. Beckham, Techno-economic analysis and life cycle assessment of a biorefinery utilizing reductive catalytic fractionation, Energy Environ. Sci, 14 (2021) 4147-4168.

[2] J.S. Luterbacher, A. Azarpira, A.H. Motagamwala, F. Lu, J. Ralph, J.A. Dumesic, Lignin monomer production integrated into the γ-valerolactone sugar platform, Energy Environ. Sci, 8 (2015) 2657-2663.

[3] Y. Wan, J.-M. Lee, Toward Value-Added Dicarboxylic Acids from Biomass Derivatives via Thermocatalytic Conversion, ACS Catal, 11 (2021) 2524-2560.

[4] V. Patil, S. Adhikari, P. Cross, H. Jahromi, Progress in the solvent depolymerization of lignin, Renew. Sust. Energ. Rev, 133 (2020) 110359.

[5] X. Ma, C. Zhang, P. Gnanasekar, P. Xiao, Q. Luo, S. Li, D. Qin, T. Chen, J. Chen, J. Zhu, N. Yan, Mechanically robust, solar-driven, and degradable lignin-based polyurethane adsorbent for efficient crude oil spill remediation, Chem. Eng. J., 415 (2021) 128956.

[6] T. Vangeel, T. Renders, K. Van Aelst, E. Cooreman, S. Van den Bosch, G. Van den Bossche, S.F. Koelewijn, C.M. Courtin, B.F. Sels, Reductive catalytic fractionation of black locust bark, Green Chem, 21 (2019) 5841-5851.

[7] Y. Liao, S.-F. Koelewijn, G.V.d. Bossche, J.V. Aelst, S.V.d. Bosch, T. Renders, K. Navare, T. Nicolaï, K.V. Aelst, M. Maesen, H. Matsushima, J.M. Thevelein, K.V. Acker, B. Lagrain, D. Verboekend, B.F. Sels, A sustainable wood biorefinery for low-carbon footprint chemicals production, Science, 367 (2020) 1385-1390.

[8] C. Huang, X. Jiang, X. Shen, J. Hu, W. Tang, X. Wu, A. Ragauskas, H. Jameel, X. Meng, Q. Yong, Lignin-enzyme interaction: A roadblock for efficient enzymatic hydrolysis of lignocellulosics, Renew. Sust. Energ. Rev, 154 (2022) 111822.

[9] X. Luo, Y. Li, N.K. Gupta, B. Sels, J. Ralph, L. Shuai, Protection Strategies Enable Selective Conversion of Biomass, Angew Chem Int Edit, 59 (2020) 11704-11716.

[10] J. Zhu, L. Chen, C. Cai, Acid Hydrotropic Fractionation of Lignocelluloses for Sustainable Biorefinery: Advantages, Opportunities, and Research Needs, ChemSusChem, 14 (2021) 3031-3046.
[11] W. Deng, L. Yan, B. Wang, Q. Zhang, H. Song, S. Wang, Q. Zhang, Y. Wang, Efficient Catalysts for the Green Synthesis of Adipic Acid from Biomass, Angew Chem Int Edit, 60 (2021) 4712-4719.
[12] S. Song, V. Fung Kin Yuen, L. Di, Q. Sun, K. Zhou, N. Yan, Integrating Biomass into the Organonitrogen Chemical Supply Chain: Production of Pyrrole and d-Proline from Furfural, Angew Chem Int Edit, 59 (2020) 19846-19850.
[13] Q. Fang, Z. Jiang, K. Guo, X. Liu, Z. Li, G. Li, C. Hu, Low temperature catalytic conversion of oligomers derived from lignin in pubescens on Pd/NbOPO4, Appl. Catal. B Environ, 263 (2020) 118325.
[14] L. Lin, X. Han, B. Han, S. Yang, Emerging heterogeneous catalysts for biomass conversion: studies of the reaction mechanism, Chem Soc Rev, 50 (2021) 11270-11292.
[15] Y.M. Questell-Santiago, M.V. Galkin, K. Barta, J.S. Luterbacher, Stabilization strategies in biomass depolymerization using chemical functionalization, Nat. Rev. Chem, 4 (2020) 311-330.
[16] X. Liu, F.P. Bouxin, J. Fan, V.L. Budarin, C. Hu, J.H. Clark, Recent Advances in the Catalytic Depolymerization of Lignin towards Phenolic Chemicals: A Review, ChemSusChem, 13 (2020) 4296-4317.
[17] T. Li, C. Chen, A.H. Brozena, J.Y. Zhu, L. Xu, C. Driemeier, J. Dai, O.J. Rojas, A. Isogai, L. Wagberg, L. Hu, Developing fibrillated cellulose as a sustainable technological material, Nature, 590 (2021) 47-56.
[18] H. Chang, E.B. Gilcher, G.W. Huber, J.A. Dumesic, Synthesis of performance-advantaged polyurethanes and polyesters from biomass-derived monomers by aldol-condensation of 5-hydroxymethyl furfural and hydrogenation, Green Chem, 23 (2021) 4355-4364.
[19] A.H. Motagamwala, K. Huang, C.T. Maravelias, J.A. Dumesic, Solvent system for effective near-term production of hydroxymethylfurfural (HMF) with potential for long-term process improvement, Energy Environ. Sci, 12 (2019) 2212-2222.
[20] S. Wang, K. Zhang, H. Li, L.P. Xiao, G. Song, Selective hydrogenolysis of catechyl lignin into propenylcatechol over an atomically dispersed ruthenium catalyst, Nat. Commun, 12 (2021) 416.
[21] L. Chen, S.-M. Luo, C.-M. Huo, Y.-F. Shi, J. Feng, J.-Y. Zhu, W. Xue, X. Qiu, 21-New insight into lignin aggregation guiding efficient synthesis and functionalization of a lignin nanosphere with excellent performance, Green Chem, 24 (2022) 285-294.
[22] F. Shu, B. Jiang, Y. Yuan, M. Li, W. Wu, Y. Jin, H. Xiao, Biological Activities and Emerging Roles of Lignin and Lignin-Based Products horizontal line A Review, Biomacromolecules, 22 (2021) 4905-4918.
[23] Y. Li, L. Shuai, H. Kim, A.H. Motagamwala, J.K. Mobley, F. Yue, Y. Tobimatsu, D. Havkin-Frenkel, F. Chen, R.A. Dixon, J.S. Luterbacher, J.A. Dumesic, J. Ralph, An “ideal lignin” facilitates full biomass utilization, Sci. Adv, 4 (2018) 9.
[24] Z.H. Liu, N. Hao, Y.Y. Wang, C. Dou, F. Lin, R. Shen, R. Bura, D.B. Hodge, B.E. Dale, A.J. Ragauskas, B. Yang, J.S. Yuan, Transforming biorefinery designs with 'Plug-In Processes of Lignin' to enable economic waste valorization, Nat. Commun, 12 (2021) 3912.
[25] L. Shuai, M.T. Amiri, Y.M. Questell-Santiago, F. Héroguel, Y. Li, H. Kim, R. Meilan, C. Chapple, J. Ralph, J.S. Luterbacher, Formaldehyde stabilization facilitates lignin monomer production during biomass depolymerization, Science, 354 (2016) 329-333.

[26] L. Shuai, B. Saha, Towards high-yield lignin monomer production, Green Chem, 19 (2017) 3752-3758.
[27] S. Van den Bosch, W. Schutyser, R. Vanholme, T. Driessen, S.F. Koelewijn, T. Renders, B. De Meester, W.J.J. Huijgen, W. Dehaen, C.M. Courtin, B. Lagrain, W. Boerjan, B.F. Sels, Reductive lignocellulose fractionation into soluble lignin-derived phenolic monomers and dimers and processable carbohydrate pulps, Energy Environ. Sci, 8 (2015) 1748-1763.
[28] M.M. Abu-Omar, K. Barta, G.T. Beckham, J.S. Luterbacher, J. Ralph, R. Rinaldi, Y. Román-Leshkov, J.S.M. Samec, B.F. Sels, F. Wang, Guidelines for performing lignin-first biorefining, Energy Environ. Sci, 14 (2021) 262-292.
[29] T. Parsell, S. Yohe, J. Degenstein, T. Jarrell, I. Klein, E. Gencer, B. Hewetson, M. Hurt, J.I. Kim, H. Choudhari, B. Saha, R. Meilan, N. Mosier, F. Ribeiro, W.N. Delgass, C. Chapple, H.I. Kenttämaa, R. Agrawal, M.M. Abu-Omar, A synergistic biorefinery based on catalytic conversion of lignin prior to cellulose starting from lignocellulosic biomass, Green Chem, 17 (2015) 1492-1499.
[30] T. Ren, S. You, Z. Zhang, Y. Wang, W. Qi, R. Su, Z. He, Highly selective reductive catalytic fractionation at atmospheric pressure without hydrogen, Green Chem, 23 (2021) 1648-1657.
[31] T.I. Korányi, B. Fridrich, A. Pineda, K. Barta, Development of 'Lignin-First' Approaches for the Valorization of Lignocellulosic Biomass, Molecules, 25 (2020) 2815.
[32] Z. Sun, G. Bottari, A. Afanasenko, M.C.A. Stuart, P.J. Deuss, B. Fridrich, K. Barta, Complete lignocellulose conversion with integrated catalyst recycling yielding valuable aromatics and fuels, Nat. Catal, 1 (2018) 82-92.
[33] M.V. Galkin, J.S. Samec, Lignin Valorization through Catalytic Lignocellulose Fractionation: A Fundamental Platform for the Future Biorefinery, ChemSusChem, 9 (2016) 1544.
[34] N. Rodriguez Quiroz, A.M. Norton, H. Nguyen, E. Vasileiadou, D.G. Vlachos, Homogeneous Metal Salt Solutions for Biomass Upgrading and Other Select Organic Reactions, ACS Catalysis, 9 (2019) 9923-9952.
[35] Y. Luo, D. Li, R. Li, Z. Li, C. Hu, X. Liu, Roles of water and aluminum sulfate for selective dissolution and utilization of hemicellulose to develop sustainable corn stover-based biorefinery, Renewable and Sustainable Energy Reviews, 122 (2020).
[36] Q. Zhai, S. Han, C.-Y. Hse, J. Jiang, J. Xu, 5-Sulfosalicylic acid as an acid hydrotrope for the rapid and green fractionation of woody biomass, Industrial Crops and Products, 177 (2022).
[37] Z. Yue, L.L. Sun, S.N. Sun, X.F. Cao, J.L. Wen, M.Q. Zhu, Structure of corn bran hemicelluloses isolated with aqueous ethanol solutions and their potential to produce furfural, Carbohydr Polym, 288 (2022) 119420.
[38] X. Xiao, J.Y. Wen, Y.Y. Wang, J. Bian, M.F. Li, F. Peng, R.C. Sun, NMR and ESI-MS spectrometry characterization of autohydrolysis xylo-oligosaccharides separated by gel permeation chromatography, Carbohyd Polym, 195 (2018) 303-310.
[39] Q. Lin, S. Liao, L. Li, W. Li, F. Yue, F. Peng, J. Ren, Solvent effect on xylose conversion under catalyst-free conditions: insights from molecular dynamics simulation and experiments, Green Chem, 22 (2020) 532-539.
[40] C. Sener, A.H. Motagamwala, D.M. Alonso, J.A. Dumesic, Enhanced Furfural Yields from Xylose Dehydration in the gamma-Valerolactone/Water Solvent System at Elevated Temperatures, ChemSusChem, 11 (2018) 2321-2331.
[41] C. Liu, L. Wei, X. Yin, X. Pan, J. Hu, N. Li, J. Xu, J. Jiang, K. Wang, Synthesis of furfural from xylan in γ-valerolactone/molten salt hydrate biphasic system, Chem. Eng. J., 425 (2021) 130608.

577 [42] C. Liu, L. Wei, X. Yin, M. Wei, J. Xu, J. Jiang, K. Wang, Selective conversion of hemicellulose
578 into furfural over low-cost metal salts in a γ-valerolactone/water solution, Ind. Crop. Prod, 147
579 (2020) 112248.
580 [43] A.H. Motagamwala, W. Won, C. Sener, D.M. Alonso, C.T. Maravelias, J.A. Dumesic, 39-
581 Toward biomass-derived renewable plastics: Production of 2,5-furandicarboxylic acid from fructose,
582 Sci. Adv, 4 (2018) 1.
583 [44] X. Luo, C. Ma, Z. Chen, X. Zhang, N. Niu, J. Li, S. Liu, S. Li, Biomass-derived solar-to-
584 thermal materials: promising energy absorbers to convert light to mechanical motion, J. Mater.
585 Chem. A, 7 (2019) 4002-4008.
586 [45] C.G. Yoo, N. Li, M. Swannell, X. Pan, Isomerization of glucose to fructose catalyzed by lithium
587 bromide in water, Green Chem, 19 (2017) 4402-4411.
588 [46] J. Tang, X. Guo, L. Zhu, C. Hu, Mechanistic Study of Glucose-to-Fructose Isomerization in
589 Water Catalyzed by $[Al(OH)_2(aq)]^+$, ACS Catal, 5 (2015) 5097-5103.
590